Temperature-Dependent Complex Indices of Refraction for Crystalline $(NH_4)_2SO_4$

M. E. Earle, R. G. Pancescu, B. Cosic, A. Y. Zasetsky, and J. J. Sloan*

Department of Chemistry, University of Waterloo, 200 University Ave. W., Waterloo, ON, Canada N2L 3G1

Received: July 24, 2006; In Final Form: September 29, 2006

We present a significantly improved set of complex indices of refraction (optical constants) for crystalline $(NH_4)_2SO_4$ at 298 K, determined from extinction spectra measured in an aerosol flow tube (AFT). The improved values provide more accurate reproductions of experimental extinction spectra when used in light scattering calculations (Mie, T-matrix, etc.). Optical constants were also derived from measurements using a cryogenic AFT at 243, 223, and 213 K, temperatures characteristic of the upper troposphere and stratosphere. Only minor changes in the optical constants were observed down to 223 K, the transition temperature to the ferroelectric phase, after which significant changes were observed. Here we report the first complex indices of refraction at reduced temperatures for both phases of crystalline $(NH_4)_2SO_4$.

1. Introduction

It is well-known that atmospheric aerosols have a significant effect on Earth's radiation budget, and consequently, on climate. Aerosol particles influence radiative transfer directly by absorbing and scattering incident short-wave (solar) radiation and long-wave (thermal) radiation from the Earth's surface. Acting as cloud condensation nuclei, aerosol particles also have an indirect radiative influence by changing cloud albedo and lifetime.[1,2] Their combined influence, which is estimated to have a net climatic cooling effect, can be quantified via remote sensing, but this requires a detailed knowledge of the optical properties of the particles as well as their phases, sizes, and chemical compositions.

Anthropogenic sulfate aerosols, which include sulfuric acid (H_2SO_4) and ammonium bisulfate and sulfate [NH_4HSO_4 and $(NH_4)_2SO_4$, respectively] are prevalent in the troposphere and contribute significantly to changes in radiative transfer.[3−6] The high scattering activity of these predominantly submicron aerosols, coupled with their abundance, can have a critical influence on climate at the local and global levels. Atmospheric modeling studies have shown that direct climate forcing due to anthropogenic sulfates contribute significantly to the cooling effect attributed to aerosols, which is comparable in magnitude with the net warming effect caused by greenhouse gases.[2,7] To improve the accuracy and predictive ability of current atmospheric radiative transfer models, it is essential that the physical and optical properties of these sulfate aerosols be well-defined.

Complex refractive indices (optical constants) for crystalline $(NH_4)_2SO_4$ at 298 K have been reported previously by Toon et al.[8] These values are widely used in remote sensing and laboratory studies of aerosols (see refs 9−12). Discrepancies observed when these optical constants are used to fit experimental extinction spectra[10] suggest that the values are not fully accurate or are too coarsely resolved. In this study, we report improved frequency dependent refractive indices for crystalline $(NH_4)_2SO_4$ at ambient pressure (1 bar) and 298 K. The new values cover the spectral range from 590 to 5990 cm^{-1} with 2 cm^{-1} resolution. In addition, we have determined optical constants with 5 cm^{-1} resolution over the same spectral range at 243 and 223 K and with 2 cm^{-1} resolution at 213 K. These lower temperatures are characteristic of the upper troposphere and stratosphere and include the ferroelectric transition near 223 K.[13−15] This transition involves structural changes in the $(NH_4)_2SO_4$ crystal lattice, which cause spontaneous polarization and also affect the complex indices of refraction strongly. Complex refractive indices of the ferroelectric phase are reported for the first time.

The new indices of refraction are based on infrared (IR) extinction measurements obtained using two different aerosol flow tubes (AFTs): a glass apparatus that was used for the room-temperature measurements and a cryogenic AFT capable of stable operation down to 150 K.[16] The indices of refraction were extracted from the measurements using a numerical procedure reported recently.[17]

2. Experimental Methods

2.1. Room-Temperature Experiments. The room-temperature experiments were carried out in the glass AFT, which is shown in Figure 1. Crystalline $(NH_4)_2SO_4$ aerosols were produced from solution using a constant output atomizer (TSI Model 3076) driven by a flow of dry N_2 (35 psi, 3 SLPM). To generate different dry aerosol sizes, five different concentrations of $(NH_4)_2SO_4$ solution were used: 0.1, 0.2, 0.5, 1, and 2 M. The solutions were prepared from reagent-grade $(NH_4)_2SO_4$ (Sigma-Aldrich Co.) and Millipore-filtered deionized distilled water.

The solution aerosols were evaporated in a diffusion dryer consisting of a tubular Nafion membrane 1 m in length and 1.8 cm i.d. (Perma Pure Inc.) enclosed in a 5 cm i.d. glass jacket. A counter-flow of dry N_2 was passed through the jacket at flow rates between 25 and 30 SLPM, producing a high relative humidity (RH) gradient that drives the rapid diffusion of gas-phase water through the Nafion membrane. Under these conditions, the RH in the aerosol stream was reduced to between 10% and 12%, drying the aerosols. The dry aerosols were then passed through a U-shaped glass tube (10 cm i.d.) pretreated with a hydrophobic fluoropolymer (FluoroPel PFC 802A-FS, Cytonix Corp.) to reduce particle deposition. The total reaction tube length, including the dryer, was approximately 3 m,

* To whom correspondence should be addressed. Phone: (519) 888-4401. Fax: (519) 746-0435. E-mail: sloanj@uwaterloo.ca.

10.1021/jp064704s CCC: $33.50
Published on Web 11/11/2006

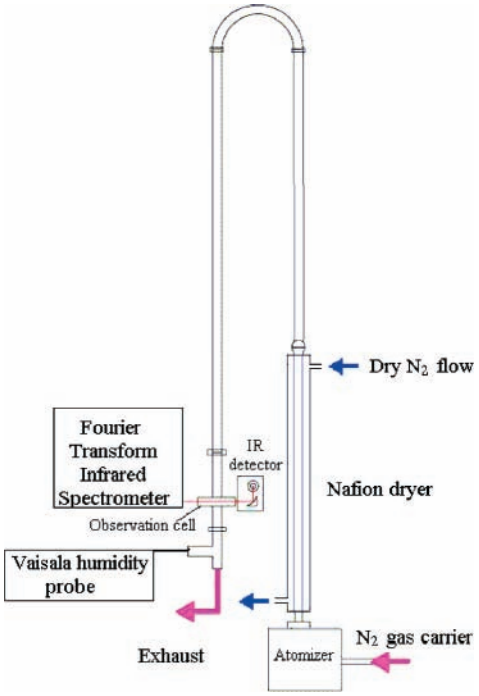

Figure 1. Glass AFT used in ambient temperature studies.

resulting in residence times on the order of 1 min. This time was sufficient for equilibration of water between the aerosol and vapor phases, as verified by a number of experiments carried out using longer residence times. The equilibrated aerosols were introduced into a stainless steel observation cell (5 cm i.d.) with two optical ports equipped with 3 cm diameter KRS-5 windows. The windows were purged with a small flow of N_2 (less than 1% of the total flow rate) to minimize aerosol deposition.

Extinction spectra were acquired by passing modulated, collimated radiation from a Fourier transform infrared (FTIR) spectrometer (Bruker IFS-55) through the observation cell and focusing it onto a mercury cadmium telluride (MCT) detector. Spectra were collected over the range from 500 to 6000 cm^{-1} at a resolution of 4 cm^{-1}, with each spectrum being an average of 100 scans. All spectra were taken under steady-state conditions, that is, after the relative humidity reached a constant value in time. The relative humidity in the observation cell was determined using a calibration curve obtained in a separate experiment, in which the area of the 1887−1891 cm^{-1} water vapor band was correlated to the relative humidity measured by a humidity probe (Vaisala Model HM70). Taking into account the uncertainties of the humidity probe readings (±1%) and calibration fits, the precision of the humidity measurements is estimated to be ±2%. Following humidity determination, water vapor spectra were routinely subtracted to obtain pure aerosol spectra.

The configuration described above and shown in Figure 1 was modified for a series of experiments in which aerosols were sampled for analysis by scanning electron microscopy (SEM). For this application, aerosols were collected on an alumina probe placed in the center of the flow tube, 3 cm below the observation cell. The aerosols in this case were produced from 0.1, 2, and 3.5 M solutions. Sampling times varied between 45, 15, and 10 min, respectively. To minimize particle agglomeration in the sample, a drying unit containing hygroscopic KOH pellets was added downstream from the Nafion dryer, reducing the relative humidity of the aerosols to 6%.

2.2. Reduced-Temperature Experiments. The low-temperature studies were carried out in a cryogenic AFT apparatus, shown schematically in Figure 2. The details of this apparatus have been described elsewhere.[16] It is comprised of four copper sections, separated by thin-walled stainless steel bellows and enclosed within an evacuated stainless steel jacket. The bottom section is equipped with optical ports for spectroscopic observation. Each copper section is equipped with cooling coils through which liquid and/or cold gaseous N_2 is passed. Section temperatures can be independently set, monitored, and controlled between room temperature and about 150 K, using a control system integrating a National Instruments I/O interface and LabView code. The approximate temperature of each section is first set by adjusting the coolant flow using a manual valve. Thereafter, the temperature is controlled by a feedback loop

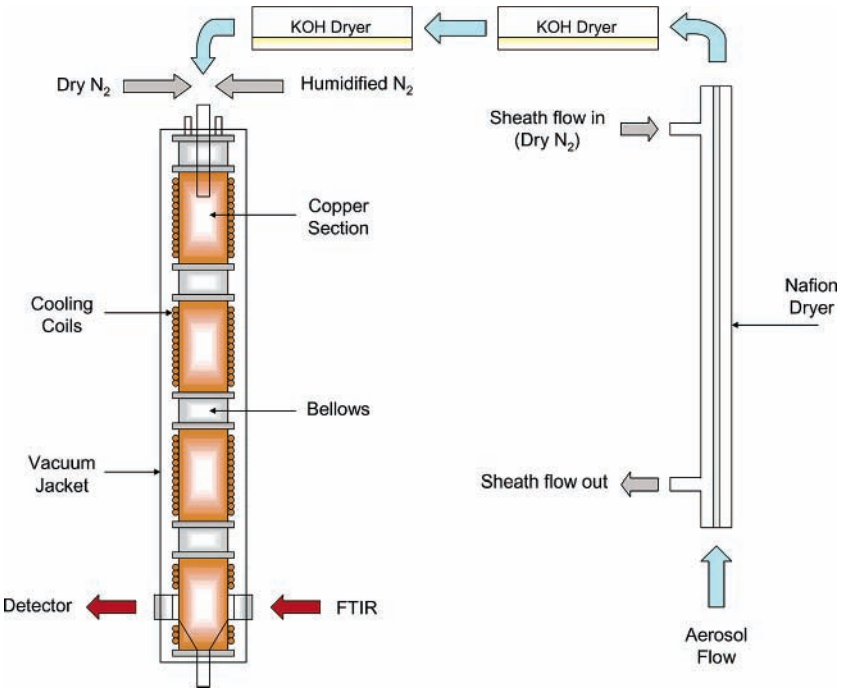

Figure 2. Cryogenic AFT apparatus used in reduced temperature studies.

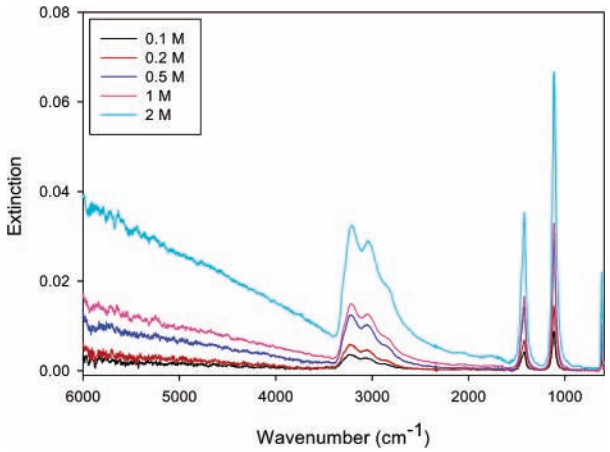

Figure 3. Extinction spectra of crystalline $(NH_4)_2SO_4$ obtained by atomizing and drying 0.1, 0.2, 0.5, 1, and 2 M aqueous solutions at 298 K.

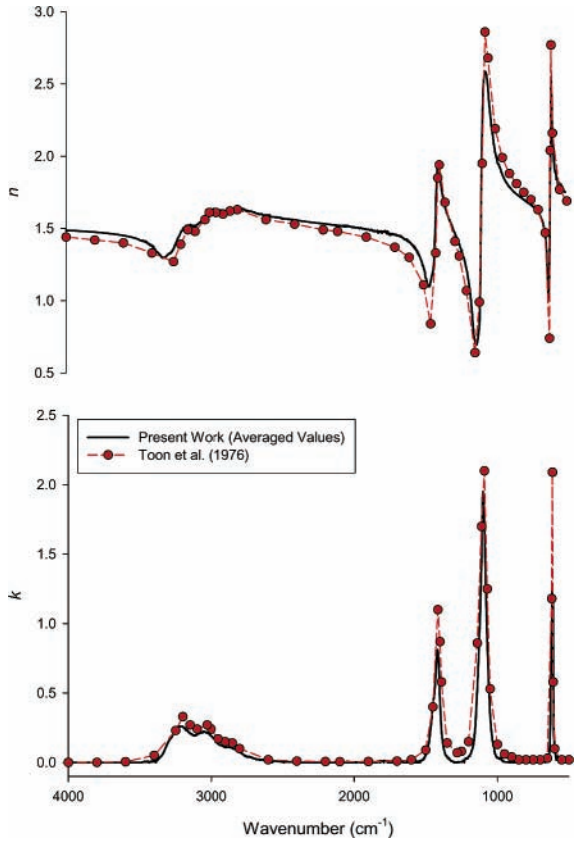

Figure 4. Comparison of our averaged optical constants obtained at 298 K with the values of Toon et al.

that monitors the temperatures measured by thermocouples attached to each section wall and adjusts the voltage applied to heaters in the coolant flow to maintain the set temperature. Experiments using $(NH_4)_2SO_4$ were conducted at 298, 243, 223, and 213 K.

The $(NH_4)_2SO_4$ aerosols were generated by atomization of aqueous solutions ranging in composition from 0.05 to 2 M $(NH_4)_2SO_4$. The aerosols were dried by passing through a 120 cm long, 1.3 cm i.d. Nafion tube enclosed within a 5 cm i.d. glass jacket, similar to that described above for the glass AFT. The aerosol leaving the dryer was then passed over hygroscopic KOH pellets, resulting in relative humidities less than 6%. The aerosol flow (typically 3 SLPM) was introduced at the top of the AFT, where it was mixed with an axial flow of carrier gas (dry N_2; typically 7 SLPM).

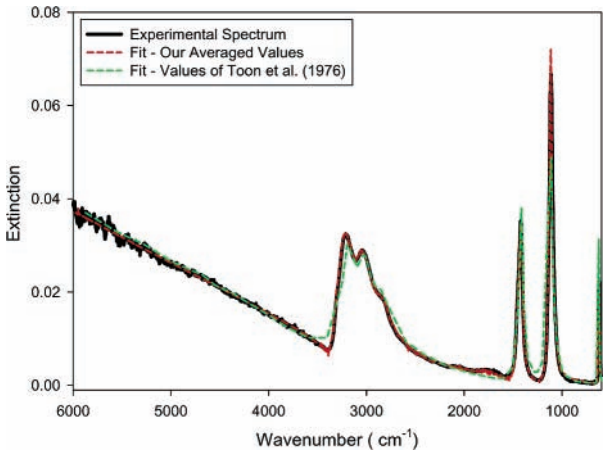

Figure 5. Calculated fits to a measured extinction spectrum of 2 M $(NH_4)_2SO_4$ at 298 K using our averaged optical constants and the values of Toon et al.

Aerosol extinction spectra were obtained by passing the IR beam from a Bruker Tensor 37 Michelson interferometer across the aerosol flow, through KRS-5 windows mounted on the bottom AFT section. After passing through the flow, the beam was focused by an off-axis parabolic mirror onto an MCT detector. Spectra were recorded over the range 460−6000 cm^{-1}, at 2 cm^{-1} resolution, using Bruker OPUS software. Pure aerosol spectra were obtained by subtracting water vapor spectra recorded at the experimental temperature.

2.3. Procedure. We used an iterative method originally proposed by Clapp et al.[18] to determine complex refractive indices from aerosol extinction measurements. The particular implementation used in this work was described previously in detail by Zasetsky et al.[17] The complex refractive indices have the form

$$n(\nu)^* = n(\nu) + ik(\nu) \quad (1)$$

where n and k are the frequency-dependent real and imaginary components, respectively. The iterative procedure requires an initial guess for the imaginary component, k, typically obtained from a small particle spectrum for which the scattering amplitude may be considered negligible. A subtractive Kramers−Kronig (KK) integration is then performed to calculate the real component, n. The KK transform also requires the "anchor point", which is the real component of the refractive index at infinite frequency, $n(\infty)$. Light scattering calculations (Mie, T-matrix, etc.) are then used to obtain extinction spectra for a number of discrete radii between 0.05 and 11.88 μm over the entire frequency range. These limits were chosen to cover the frequency and size range to which the scattered intensity is most sensitive. These extinction spectra, which we refer to as the spectral basis set, are then fit to an experimental spectrum using a linear least-squares method. The amplitudes of the monodisperse spectra that produce the best fit constitute the size distribution for the sample.[19]

The initial guess for the imaginary component is varied and the procedure is repeated in a systematic way until a minimum difference is obtained between the experimental spectrum and the fit. Any remaining, small-scale discrepancies between the experimental and calculated spectra are reconciled by correcting k by a small amount at each frequency and repeating the steps described above. The final set of scaled and corrected optical constants is then output.

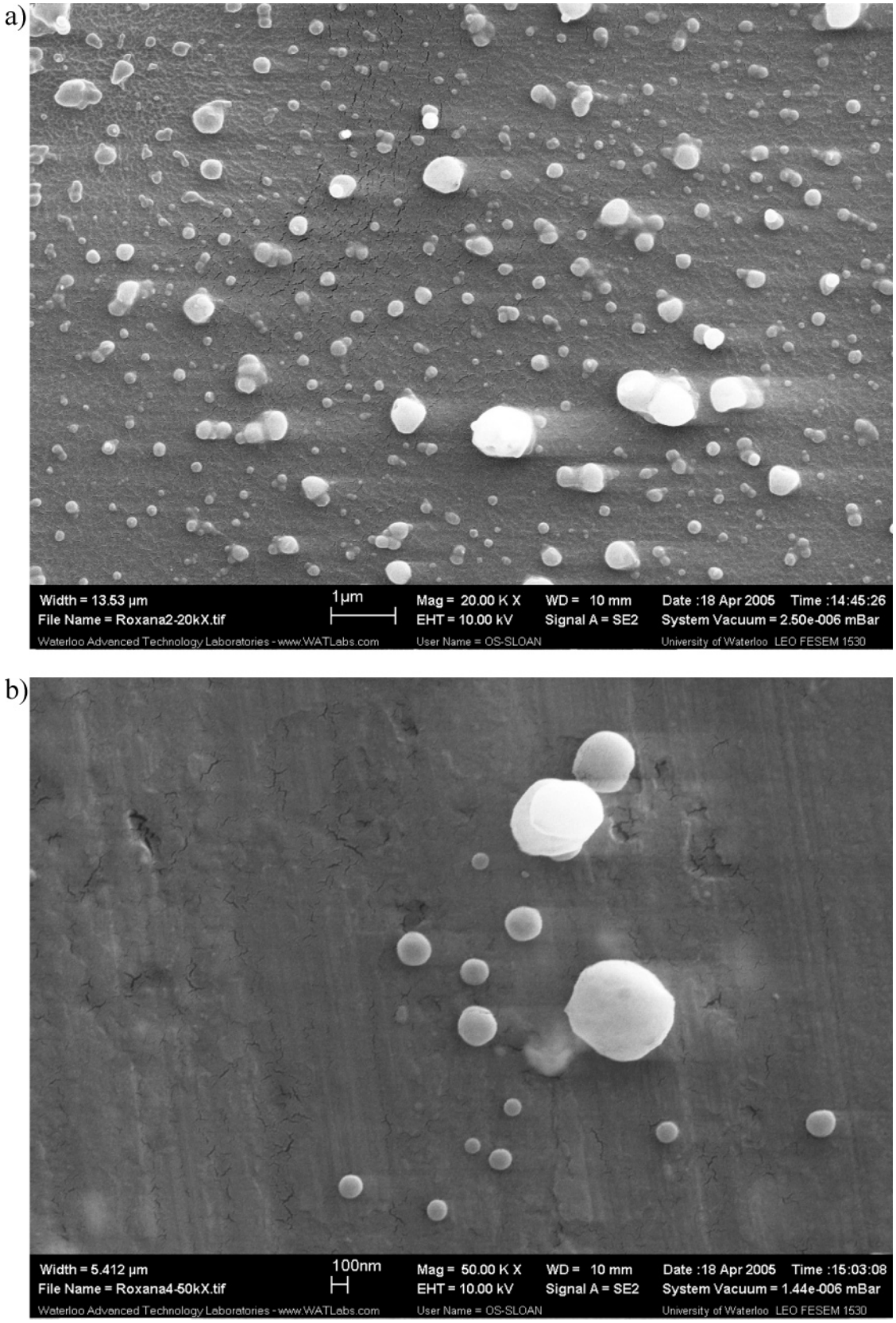

Figure 6. SEM scan of crystalline $(NH_4)_2SO_4$ obtained using (a) 0.1 M solution and 30 min sampling time at 298 K and (b) 2 M solution and 15 min sampling time at 298 K.

3. Results and Discussion

3.1. Room-Temperature Optical Constants for Crystalline $(NH_4)_2SO_4$. The infrared spectra shown in Figure 3 were obtained at 298 K using different initial concentrations of $(NH_4)_2SO_4$ solution as described in section 2.1, resulting in different dry aerosol size distributions. The strong absorption features at 2800−3300 cm^{-1}, 1420−1450, 1115, and 620 cm^{-1}, corresponding to the ν_3 (NH_4^+), ν_4 (NH_4^+), $\nu_3(SO_4^{2-})$, and $\nu_4(SO_4^{2-})$ modes, respectively,[20] are clearly visible under all conditions. As would be expected, there is an increase in aerosol

extinction with the concentration of $(NH_4)_2SO_4$ solution. The increase in extinction above 3500 cm^{-1} is due to particle scattering, which increases for larger sizes.[21]

Each extinction spectrum shown in Figure 3 was used to compute a new set of optical constants using the procedure described in section 2.3. In all cases, the spectrum that produced the smallest particles, which was obtained from the 0.1 M $(NH_4)_2SO_4$ solution, was used as an initial guess for $k(\nu)$. An anchor point of $n(\infty) = 1.528$ was adopted from the data of Koop in the visible region at room temperature.[22] The optical constants obtained from each spectrum in Figure 3 were then averaged. Figure 4 shows these averaged values plotted against the values of Toon et al.,[8] which were the only other data available before our work. Compared to our averaged values, which cover the range 590−5990 cm^{-1} with 2 cm^{-1} resolution, the values of Toon et al. are poorly resolved, with only 58 values between 500 and 6000 cm^{-1}. In addition, there are significant differences in n and k values between the two data sets. The differences in k are limited to the absorption band regions, while the differences in n cover most of the spectral range. As a result, the values of Toon et al. are insufficient to accurately reproduce $(NH_4)_2SO_4$ extinction spectra, explaining the fitting errors observed previously.[10] This is demonstrated in Figure 5, which shows that a measured $(NH_4)_2SO_4$ spectrum is reproduced exactly using our averaged optical constants, whereas the optical constants of Toon et al. do not give as good a fit to the measured spectrum.

The good agreement between experimental and calculated spectra using the new optical constants suggests that the use of Mie theory in the numerical fitting procedure is appropriate, and hence, that the assumption of spherical particles is valid. To further support this assumption, solid $(NH_4)_2SO_4$ aerosols were imaged using SEM. Figure 6a,b shows SEM images of samples collected to show the particle morphology under different conditions during the course of this work. These show that under the experimental conditions used in this work, the aerosols were indeed spherical or near-spherical, which is consistent with the findings of previous studies of crystalline $(NH_4)_2SO_4$ particles.[23,24]

3.2. Reduced Temperature Optical Constants for Crystalline $(NH_4)_2SO_4$. Extinction spectra of crystalline $(NH_4)_2SO_4$ were measured in the cryogenic AFT (see section 2.2) at 298, 243, 223, and 213 K. The changes in spectral features with decreasing temperature are shown in Figure 7a. With decreasing temperature, the shoulder on the $\nu_3(NH_4^+)$ mode at 3300 cm^{-1} becomes more distinct and sharp, while the diffuse peak at approximately 3062 cm^{-1} increases in intensity with respect to the other features in the band.

The ferroelectric transition below 223 K is signified by changes in the $\nu_4(SO_4^{2-})$ peak centered at about 1130 cm^{-1} and the $\nu_1(SO_4^{2-})$ feature at approximately 975 cm^{-1}. In the former, two shoulders develop on either side of the central peak, which itself shifts to lower wavenumbers (Figure 7b). In the latter, significant enhancement is observed, along with a shift to lower wavenumbers (Figure 7c). The enhancement is believed to arise from distortions of the SO_4^{2-} molecule, as the $\nu_1(SO_4^{2-})$ mode is forbidden for perfect tetrahedral geometry.[13] The temperature-dependent spectral changes detailed above are in accordance with those documented previously.[13,15]

The numerical procedure detailed in section 2.3 was used to determine the real and imaginary indices of refraction from the extinction spectra. T-matrix theory, which assumes aspherical (spheroid) particles,[25] was used instead of Mie theory for light-scattering calculations. The use of T-matrix calculations,

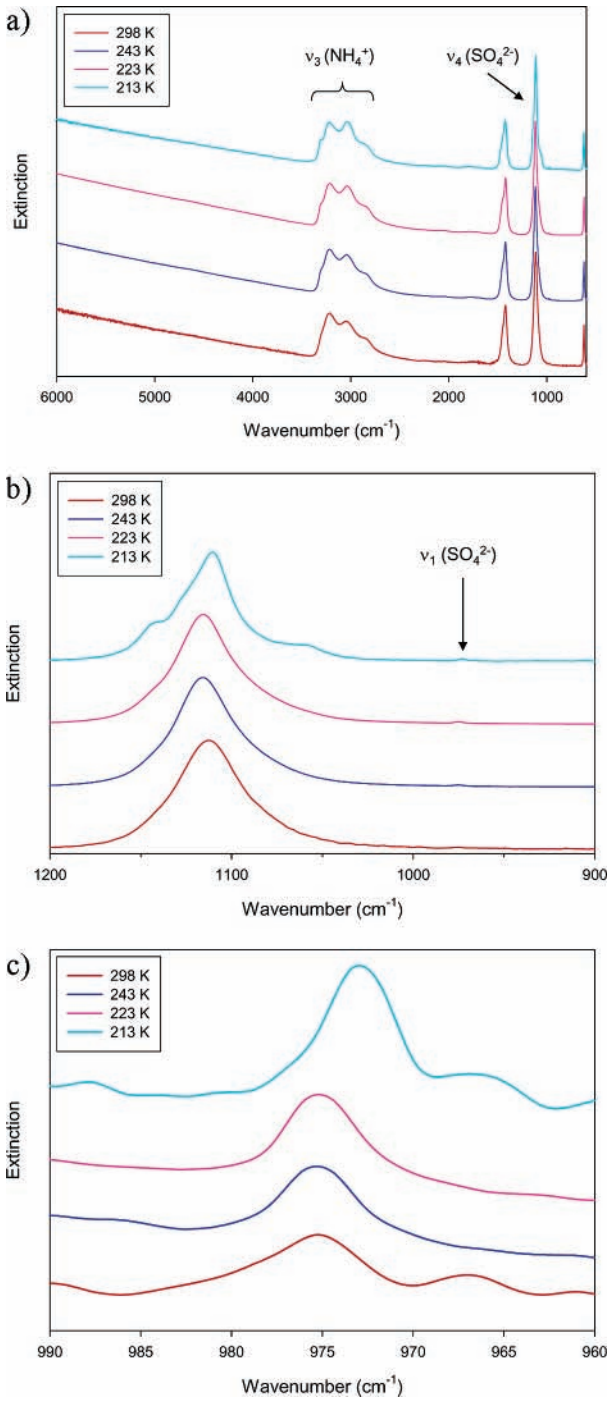

Figure 7. (a) Changes in extinction spectra of crystalline $(NH_4)_2SO_4$ (from 1 M solution) as a function of temperature, (b) expanded view of the $\nu_4(SO_4^{2-})$ feature, and (c) expanded view of the $\nu_1(SO_4^{2-})$ feature. Spectra are scaled and offset for clarity.

employing spheroid aspect ratios between 0.7 and 1.4, gave better-calculated fits to experimental spectra within the procedure and more accurate refractive indices. As shown in Figure 6a,b, the majority of crystalline $(NH_4)_2SO_4$ particles are not perfectly spherical but near-spherical. Clapp et al. have shown that Mie calculations for similar small particles (ammonia aerosols) are highly shape-dependent, with absorption features shifting due to surface resonance.[26] We note that the calculations employing aspherical particles are more appropriate for characterizing any aspherical (solid) particles or agglomerates that may form.

The averaged indices of refraction determined at 298 K in the glass AFT (section 3.1) were used as an initial guess for

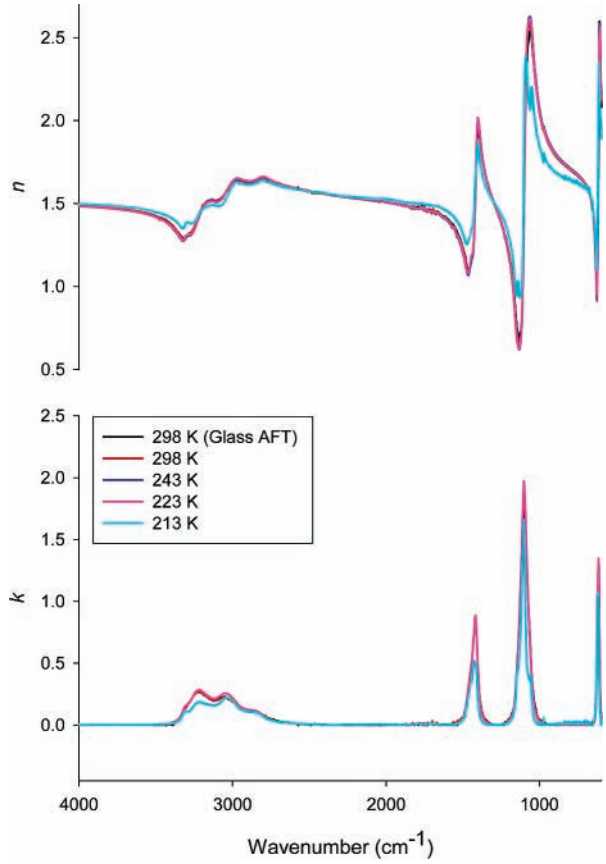

Figure 8. Temperature-dependent refractive indices of crystalline $(NH_4)_2SO_4$ obtained from glass and cryogenic AFTs.

the values obtained at 298, 243, and 223 K in the cryogenic AFT. Given the significant changes in crystalline $(NH_4)_2SO_4$ spectra beyond the ferroelectric transition at 223 K, it was necessary to obtain a new initial guess from a nonscattering spectrum of small particles at 213 K. These small particles were generated by atomizing and drying a highly dilute solution of $(NH_4)_2SO_4$ (0.02 M), and values of *k* were determined from IR extinction spectra using the approach of Dohm et al.[27] The resulting temperature-dependent complex refractive indices are plotted in Figure 8, along with the averaged values obtained in the glass AFT. There are only minor variations in *n* and *k* down to 223 K, but at 213 K, distinct changes are observed, due to the paraelectric-to-ferroelectric transition. Figure 9a shows calculated fits to an extinction spectrum measured at 213 K using optical constants obtained at 298 and 213 K, respectively. The improved fit obtained using the 213 K values is visible in the $\nu_3(NH_4^+)$ region. An expanded view is given in Figure 9b, which shows more clearly the improved fit obtained using the 213 K values in the $\nu_4(SO_4^{2-})$ region, which undergoes the most significant changes following the ferroelectric transition.

Frequency-dependent uncertainties for the real and imaginary indices of refraction were estimated at each temperature using the statistical approach of Dohm et al.[27] The uncertainties are greatest in the absorption band regions. At room temperature, errors in *n* and *k* are typically 6% or smaller. As the temperature is reduced to 243 and 223 K, errors in *n* are below 4%, while those in *k* are below 5%. This decrease in uncertainty can be attributed to the improvement in signal-to-noise ratio in the extinction spectra at lower temperatures. Contrary to this, errors in *n* and *k* at 213 K are typically less than 6% and 8%, respectively. We attribute the increased error in this case to the lower signal-to-noise ratio in the small particle spectra used to derive the "initial guess" optical constants at this temperature.

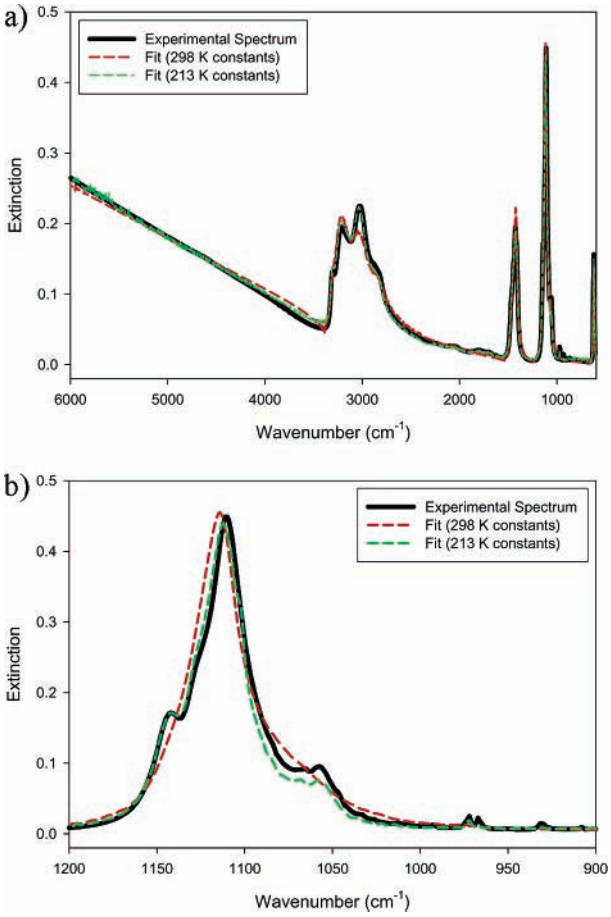

Figure 9. (a) Calculated fits to an extinction spectrum of crystalline $(NH_4)_2SO_4$ (from 2.1 M solution) at 213 K using optical constants determined at 298 and 213 K and (b) expanded view showing fitting in region of $\nu_4(SO_4^{2-})$ feature.

Finally, we note that the averaged refractive indices obtained at 298 K from the glass AFT studies using Mie theory and the values obtained at the same temperature from the cryogenic AFT studies using T-matrix theory are consistent. Frequency-dependent differences in *n* and *k* between the two data sets are within experimental uncertainties except for a small difference in the region of the 600 cm^{-1} SO_4^{2-} band, which we attribute to noise in the measurements. Thus, both methods seem appropriate in the case of mostly spherical and near-spherical particles. T-matrix theory should be used when any larger deviations from sphericity are present.

4. Conclusions

The preexisting complex refractive indices of crystalline $(NH_4)_2SO_4$ obtained at 298 K by Toon et al., though widely used, are inadequate to reproduce experimental extinction spectra accurately. We have determined a new set of optical constants at 298 K that better reproduce extinction features in $(NH_4)_2SO_4$ spectra, owing to more accurate, higher resolution values. We have also determined the first refractive indices of crystalline $(NH_4)_2SO_4$ at lower, atmospherically relevant temperatures, 243, 223, and 213 K. Only minor temperature dependent changes in the optical constants are observed from room temperature down to 223 K. Below 223 K, however, crystalline $(NH_4)_2SO_4$ undergoes a ferroelectric transition, giving rise to significant changes in the indices of refraction.

These new indices of refraction are intended for use in remote sensing and laboratory studies of solid $(NH_4)_2SO_4$ at tempera-

tures lower than 223 K. The differences in the indices of refraction for the two solid phases are large enough to permit their identification in laboratory measurements having high signal-to-noise ratios. It would not, however, be possible to distinguish between them in atmospheric remote sensing measurements using current technology, because in this case, gas-phase interference would obscure the spectral differences.

Acknowledgment. This research was supported by Natural Sciences and Engineering Research Council of Canada, the Canadian Foundation for Climate and Atmospheric Studies, and the Ontario Research and Development Challenge Fund. The authors also wish to thank Monica Harvey for assistance with extinction measurements.

Supporting Information Available: Averaged complex refractive indices for crystalline $(NH_4)_2SO_4$ at 298, 243, 223, and 213 K. This material is available free of charge via the Internet at http://pubs.acs.org.

References and Notes

(1) Charlson, R. J.; Langner, J.; Rodhe, H.; Leovy, C. B.; Warren, S. G. *Tellus* **1991**, *43A*, 152−163.

(2) Charlson, R. J.; Schwartz, S. E.; Hales, J. M.; Cess, R. D.; Coakley, J. A.; Hansen, J. E.; Hofmann, D. J. *Science* **1992**, *255*, 423−430.

(3) Sheridan, P. J.; Brock, C. A.; Wilson, J. C. *Geophys. Res. Lett.* **1994**, *21*, 2587−2590.

(4) Talbot, R. W.; Dibb, J. E.; Loomis, M. B. *Geophys. Res. Lett.* **1998**, *25*, 1367−1370.

(5) Warneck P. *Chemistry of the Natural Atmosphere*; Academic Press: San Diego, CA, 2000; pp 587−655.

(6) Martin, S. T.; Hung, H. M.; Park, R. J.; Jacob, D. J.; Spurr, R. J. D.; Chance, K. V.; Chin, M. *Atmos. Chem. Phys.* **2004**, *4*, 183-214.

(7) Kiehl, J. T.; Briegleb, B. P. *Science* **1993**, *260*, 311−314.

(8) Toon, O. B.; Pollack, J. B.; Khare, B. N. *J. Geophys. Res.* **1976**, *81*, 5733−5748.

(9) Cziczo, D. J.; Abbatt, J. P. D. *J. Geophys. Res.* **1999**, *104*, 13781−13790.

(10) Han, J. H.; Martin, S. T. *Aerosol Sci. Technol.* **2001**, *34*, 363−372.

(11) Hung, H. M.; Martin, S. T. *Appl. Spectrosc.* **2002**, *56*, 1067−1081.

(12) Onasch, T. B.; Siefert, R. L.; Brooks, S. D.; Prenni, A. J.; Murray, B.; Wilson, M. A.; Tolbert, M. A. *J. Geophys. Res.−Atmos.* **1999**, *104*, 21317−21326.

(13) Fortin, T. J.; Shilling, J. E.; Tolbert, M. A. *J. Geophys. Res.* **2002**, *107*.

(14) Matthias, B. T.; Remeika, J. P. *Phys. Rev.* **1956**, *103*, 262.

(15) Chelf, J. H.; Martin, S. T. *J. Geophys. Res.* **2001**, *106*, 1215−1226.

(16) Khalizov, A.; Earle, M. E.; Johnson, W. J. W.; Stubley, G. D.; Sloan, J. J. *Rev. Sci. Instrum.* **2006**, *77*.

(17) Zasetsky, A. Y.; Khalizov, A. F.; Earle, M. E.; Sloan, J. J. *J. Phys. Chem. A* **2005**, *109*, 2760−2764.

(18) Clapp, M. L.; Miller, R. E.; Worsnop, D. R. *J. Phys. Chem.* **1995**, *99*, 6317−6326.

(19) Zasetsky, A. Y.; Khalizov, A. F.; Sloan, J. J. *Appl. Opt.* **2004**, *43*, 5503−5511.

(20) Socrates, G. *Infrared and Raman Characteristic Group Frequencies: Tables and Charts*, 3rd ed.; Wiley: New York, 2001.

(21) Weis, D. D.; Ewing, G. E. *J. Geophys. Res.* **1996**, *101*, 18709−18720.

(22) Koop, T. Personal communication.

(23) Brooks, S. D.; Garland, R. M.; Wise, M. E.; Prenni, A. J.; Cushing, M.; Hewitt, E.; Tolbert, M. A. *J. Geophys. Res.* **2003**, *108*.

(24) Dick, W. D.; Ziemann, P. J.; Huang, P. F.; McMurry, P. H. *Meas. Sci. Technol.* **1998**, *9*, 183−196.

(25) Borrmann, S.; Luo, B. P.; Mishchenko, M. *J. Aerosol Sci.* **2000**, *31*, 789−799.

(26) Clapp, M. L.; Miller, R. E. *Icarus* **1993**, *105*, 529−536.

(27) Dohm, M. T.; Potscavage, A. M.; Niedziela, R. F. *J. Phys. Chem. A* **2004**, *108*, 5365−5376.